Experimental Verification of Capillary Force and Water Retention between Uneven-Sized Spheres

Ning Lu[1]; Jeremy Lechman[2]; and Kelly T. Miller[3]

Abstract: The recently established theoretical results of the solid-water characteristic curve (SWCC) and capillary force characteristic curve (CFCC) are experimentally verified for mechanical and hydrologic interaction between uneven-sized spherical particles under partially saturated conditions. It is shown that the theoretical framework, based on the minimization of the free energy of the liquid meniscus between the two uneven-sized particles, can predict both water retention and capillary force accurately for spherical particles ranging in radius from 165 to 252 μm. The experimental technique is novel and the results at such scale are valuable for the understanding of gas-solid-liquid interaction among granular media, since there is very limited experimental data available in the literature. The comparisons between the theoretical and experimental predictions of the SWCC and CFCC indicate that the agreements are generally very good, confirming the validity of the theory.

DOI: 10.1061/(ASCE)0733-9399(2008)134:5(385)

CE Database subject headings: Absorption; Interfacial tension; Unsaturated soils; Granular materials; Tensile stress; Experimentation; Verification.

Introduction

Capillary forces in soils play an important role in soil's mechanical and hydrologic behavior. For example, their occurrence can increase the strength of soils appreciably. An accurate description of capillary force in terms of thermodynamic variables and soil particle and pore size distributions is important for understanding of the stress state in partially saturated soils, which is directly related to their strength and deformation. For a given soil, the capillary force among soil particles is a function of soil-water content; therefore, this function is called the capillary force characteristic curve (CFCC). For a given soil, the water content is a function of environmental variables such as relative humidity or the matric suction; therefore, this function is called the solid-water characteristic curve (SWCC).

Both the CFCC and SWCC can be assessed by the thermodynamic equilibrium principle applied to gas-liquid-solid phase boundaries among soil particles, and at the most fundamental level, the liquid bridge between two uneven-sized particles.

In the two-particle system shown in Fig. 1, the dashed lines in Fig. 1(a) represent a water lens that has condensed onto the particles with the geometry indicated by the principal radii of curvature r_1 and r_2. It is these local radii of curvature that determine the mean curvature and thus the pressure difference across the liquid-air interface, i.e., the matric suction. If the interface is viewed macroscopically, so that its thickness can be considered to be negligible and the surface tension can be said to be uniform and acting along the interface, it makes no difference whether one approaches the problem from the direction of the mechanical equilibrium of the interface, the minimization of the free energy (an equivalent statement of force balance if there is no energy dissipation due to viscosity), or the thermodynamics of surface excess quantities (e.g., Miller and Neogi 1985). The fundamental relationship is the Laplace equation

$$u_a - u_l = 2H\sigma_{\mathrm{la}} \tag{1}$$

where u_a and u_l=pressures of the air and liquid phases, respectively; $H=1/2(1/r_1+1/r_2)$=mean curvature with sign depending on the concavity or convexity of the meniscus surface; and σ_{la}=liquid-air surface tension.

The problem of the shape of the water meniscus between two spheres will reduce to Eq. (1) when the minimum of the correct free energy functional is found with the appropriate boundary conditions. Considered here is a system with constant temperature, total volume, and total mole number of fluid particles. The appropriate free energy is then the Helmholtz free energy which, in cylindrical coordinates [see Figs. 1(b and c)], and considering only the left particle (in Fig. 1) for illustration (the free energy of the bottom half can be expressed in the same manner), has the functional form (e.g., De Bisschop and Rigole 1982)

$$F[r(z)] = 2\pi\sigma_{\mathrm{la}}\int_0^{z_c} r(1+\dot{r}^2)^{1/2}dz - \Delta u\left[\pi\int (r^2-g^2)dz - V_t\right] + 2\pi(\sigma_{\mathrm{ls}}-\sigma_{\mathrm{sa}})\int g(1+\dot{g}^2)^{1/2}dz + \sigma_{\mathrm{sa}}\frac{4\pi R_1^3}{3} \tag{2}$$

where the subscripts l, a, and s=liquid, air, and solid phases present respectively, and the symbol $\bullet$=spatial derivative d/dz.

[1]Professor, Division of Engineering, Colorado School of Mines, Golden, CO 80401 (corresponding author). E-mail: ninglu@mines.edu

[2]Formerly, Graduate Student, Scientist Dept. of Surface and Interface Sciences, Sandia National Laboratories, P.O. Box 5800, Mail Stop 1415, Albuquerque, NM 87185-1415.

[3]Research Assistant Professor, Dept. of Chemical Engineering, Colorado School of Mines, Golden, CO 80401.

Note. Associate Editor: Ching S. Chang. Discussion open until October 1, 2008. Separate discussions must be submitted for individual papers. To extend the closing date by one month, a written request must be filed with the ASCE Managing Editor. The manuscript for this paper was submitted for review and possible publication on February 13, 2006; approved on September 18, 2007. This paper is part of the ***Journal of Engineering Mechanics***, Vol. 134, No. 5, May 1, 2008. ©ASCE, ISSN 0733-9399/2008/5-385–395/$25.00.

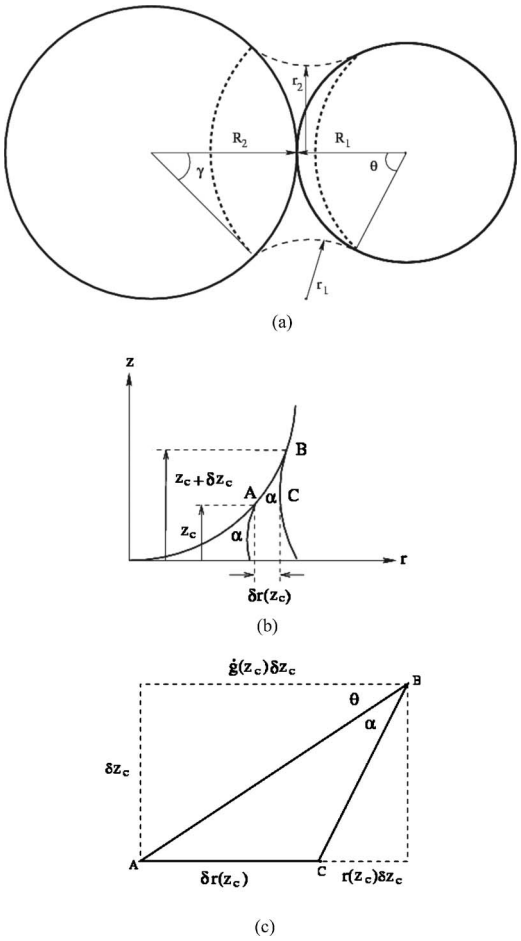

Fig. 1. Illustration of meniscus between two uneven-sized particles: (a) definition of geometry; (b) variation of meniscus-particle contact as result of variation of profile; and (c) closeup of curvature triangle created by points A, B, and C

The pressure difference across the liquid-air interface, Δu, plays the role of the Lagrange multiplier on the constant volume constraint, and the total volume of the condensed lens is V_t. The function, $g=g(z)$, defines the particle surface while the limit of integration z_c=point of contact between the particle surface and the meniscus profile [Fig. 1(c)]. It should be noted that Eq. (2) represents a variable end-point problem of the calculus of variations. This means that, as one would expect experimentally, there is only one independent variable. The Lagrange multiplier (matric suction, Δu), volume of the liquid, V_t, and end point, z_c, are related to one another so that specifying one implies the others; although the matric suction end-point relationship may not be single valued (Orr et al. 1975), stability considerations or knowing the volume of the liquid will sort this out. In the present work, the volume of the liquid is the control variable while the matric suction and end point are free to find their values in accordance with the minimum free energy of the functional in Eq. (2).

Several approaches to solving the Laplace equation for the shape of the liquid meniscus between two particles can be found in the literature. Many are concerned with the meniscus between two identical particles (e.g., Melrose 1966; Erle et al. 1971; De Bisschop and Rigole 1982). Lian et al. (1993) in particular develop a numerical technique to solve the Laplace equation for two equal-sized particles and compare it to the so-called toroidal approximation, which assumes the meniscus profile to be circular,

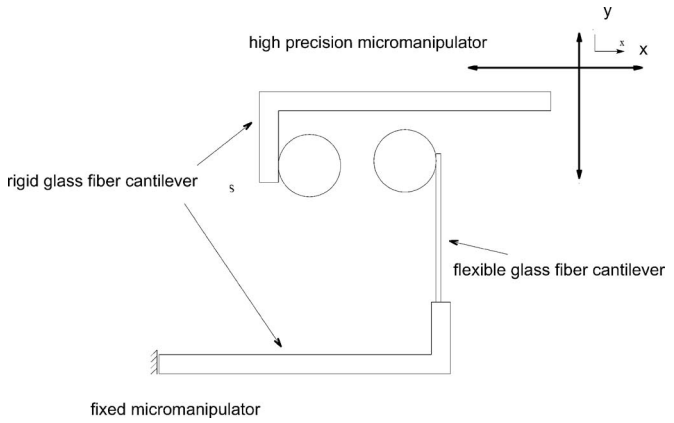

Fig. 2. Schematic diagram of experimental apparatus

for determining the capillary force. They find errors of less than 10% between the numerical solution and the approximation. They find that both their numerical method and the toroidal approximation underestimate experimentally determined forces at small particle separations and large liquid volumes. They also determine a simple relationship between the liquid volume and critical distance between particles when the liquid bridge ruptures. Molenkamp and Nazemi (2003) also consider equal-sized, rough particles. They develop a numerical approach to solving the Laplace equation and compare it to the toroidal approximation with similar results.

Orr et al. (1975) solved the general problem of a sphere in contact with a plane of arbitrary liquid-solid contact angle. This solution can be used to model even-sized spheres with an angle of $\pi/2$, or uneven-sized spheres with an arbitrary angle. Their tables of analytic solutions provide the basis for assessing the validity of the toroidal approximation for uneven spheres (Lechman and Lu 2008). It was shown that as the particles become increasingly different in size the toroidal approximation

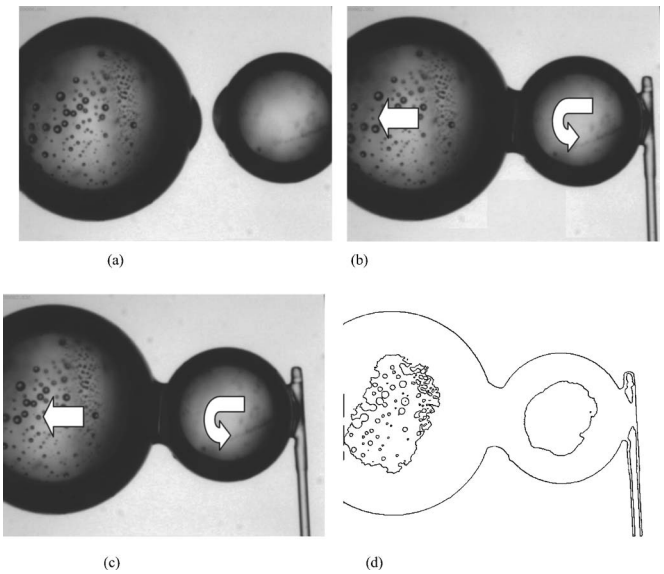

Fig. 3. Example frames from typical movie: (a) before particles are engaged; (b) just before separation; (c) just after separation; and (d) results of LoG edge-finding technique on stage (c)

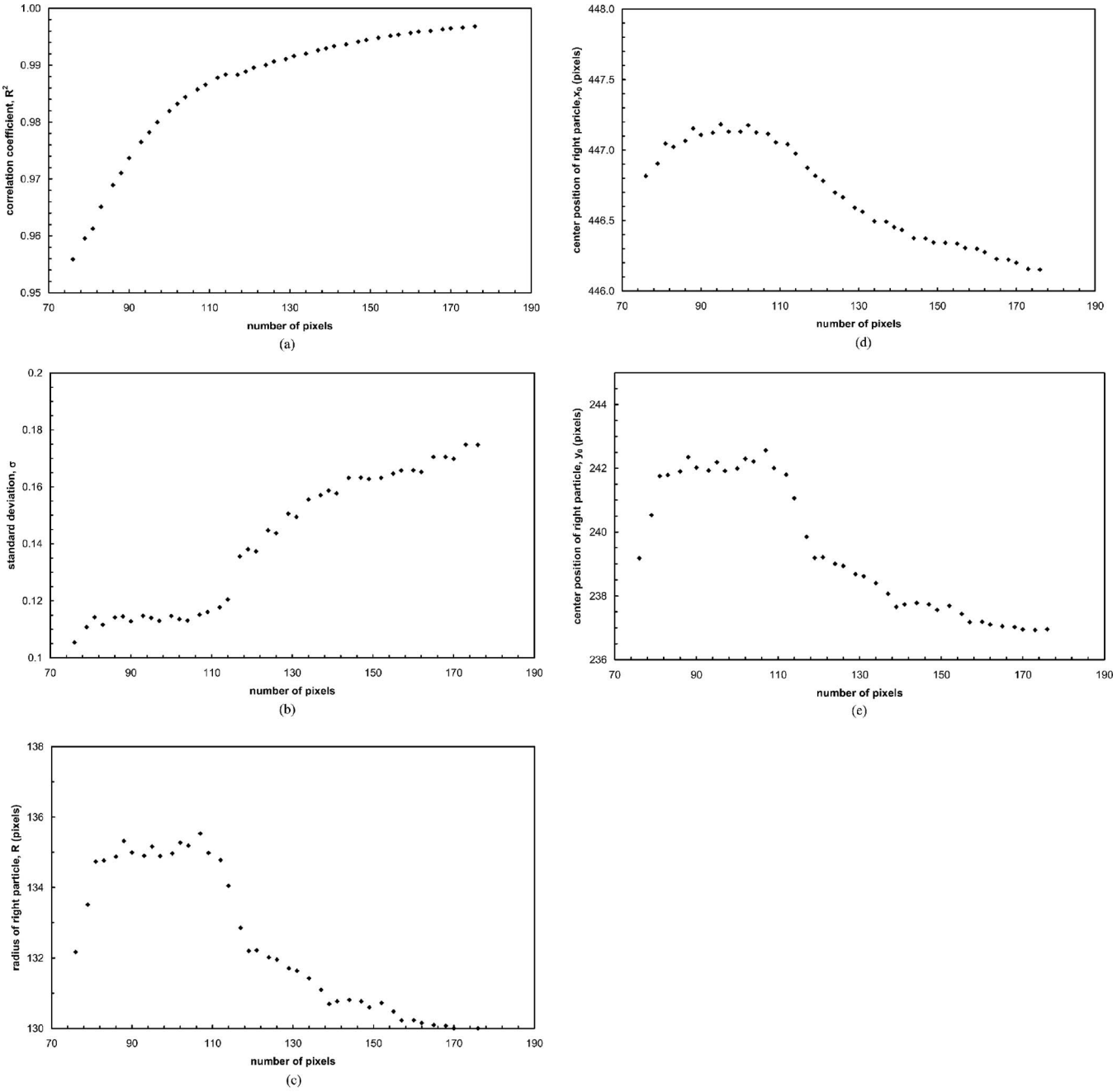

Fig. 4. Results of fitting equation of circle to right particle in Fig. 3 for different numbers of pixel data used in fit: (a) correlation coefficient, R^2, as function of number of pixels used in fit; (b) standard error in fit as function of number of pixels used; (c) radius of particle found from curve fitting; (d) value of z coordinate at center of particle; and (e) value of r coordinate at center of particle

becomes increasingly errant. However, the question remains as to how well the theory of Orr et al. captures physical reality.

Experimental investigations of the capillary force between spheres and plates and two spheres have a long history. McFarlane and Tabor (1950) investigated the role of humidity on the adhesion between a sphere and a plate. They found that the adhesion for very small film thicknesses and small contact angles, α, can be described by the relation

$$F_{\text{cap}} = 4\pi R\sigma_{\text{la}} \cos \alpha \tag{3}$$

where R=radius of the particle. Mason and Clark (1965) developed a technique to measure small capillary forces over a range of particle separations. Their results show that the capillary force reaches a maximum at small separation and decreases until rupture of the liquid bridge occurs. Mathewson (1988) investigated the effect of viscous forces during the separation of a sphere and a plate. Pepin et al. (2000a,b) investigate the evolution of the liquid bridge up to rupture and develop a model to predict the shape and rupture distance. Rossetti et al. (2003) investigate the rupture energy of liquid bridges between glass spheres of dissimilar energy and find that particle wettability affects both the geometry and capillary pressure of the liquid bridge.

In the current work, an experimental program is developed to assess the theoretical results for the capillary force between

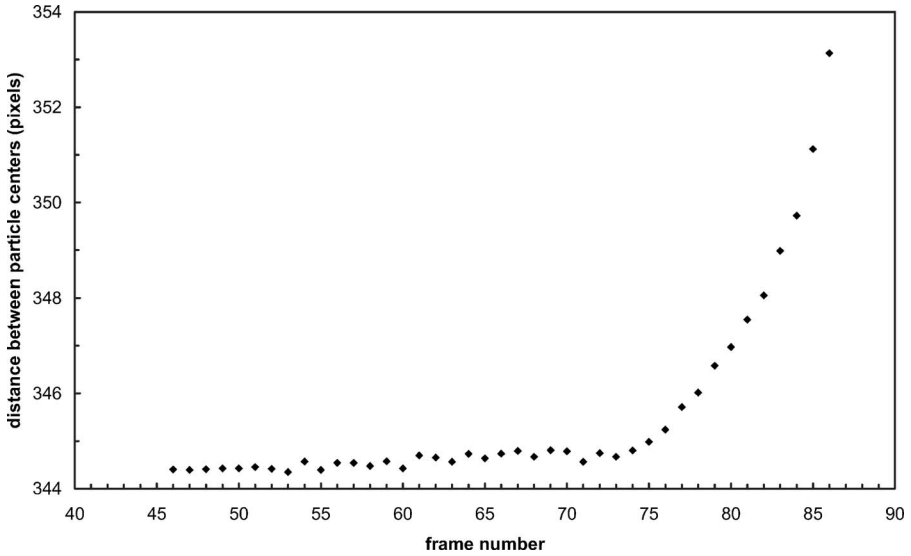

Fig. 5. Distance between particle centers for various frames. Error bars represent estimated error of about 1.12% in measured value of distance between particle centers.

uneven-sized particles in contact with a liquid meniscus between them, which was presented in a previous work (Lechman and Lu 2008).

Experimental Setup

Equipment and Materials

A micromechanical testing technique developed by Eccleston and Miller (2002), for measuring particle-particle adhesion forces, is adapted for measurement of capillary bridge forces. In the present application of this method, shown schematically in Fig. 2, a glass sphere with diameter in the hundreds of microns is glued to a glass fiber cantilever while another is glued to a rigid capillary tube. A small drop of liquid is applied to one of the spheres, and the capillary force is measured by the deflection of the fiber cantilever as the particles are brought together and separated. The position of the base of the particle-cantilever is fixed, while the movement of the particle attached to the rigid capillary tube is controlled by a high precision micromanipulator. Positions and displacements are tracked using digital video microscopy under an inverted light microscope. Image processing techniques are used to analyze the images taken during the experiments.

As mentioned, the cantilever is a glass fiber cylinder of about 30 μm diameter. For small lateral deflections the bending stiffness can be determined from beam theory as

$$k_b = \frac{3\pi E r^4}{4L^3} \tag{4}$$

where E=Young's modulus for glass, taken to be the commonly used value of 70 GPa (e.g., Forsyth 2003); r=radius of the fiber; and L=its length. For the results presented here, dimensional measurements determined the value of the cantilever stiffness to be 0.327 N/m ± 7.25%. The cantilever force is then given by the displacement of the particle from its at-rest position multiplied by the beam stiffness. The force of interest here is the force required to separate particles, which were initially in contact. In general, the capillary force is a function of particle separation (Mason and Clark 1965); however, viscosity effects can be ignored if one considers only the force required to separate contacting particles (Mathewson 1988). Also, the effects of advancing and receding contact angles and meniscus particle contact point slippage or pinning can be minimized since deformation of the meniscus is minimized (Pepin et al. 2000a, Rosetti et al. 2003). Figs 3(a–c) show several frames of a typical movie when the particles are separated [Fig. 3(a)], just before particle separation [Fig. 3(b)], and just after separation [Fig. 3(c)]. For reference, a frame is captured every 1/30 s. In the consequent analysis, for simplicity, the effects of viscosity and contact angle hysteresis are not quantified.

Rough glass spheres (note the pock marks and bubbles in the particles in Fig. 3) ranging in diameter from about 320 to 650 μm were used in the experiments and glycerol, chosen for its low volatility, was used as the liquid binder. The particle size ratios in the experiments were 1:1, 1.22:1, and 1.56:1. The surface tension of glycerol in air was found from tabulated values to be about 0.063 N/m (Washburn 2003).

Testing Procedure

The experiment consisted of applying a drop of glycerol to the rigidly bound particle and bringing it in contact with the cantilever particle. The particles were brought together and separated several times to ensure uniformity of liquid coverage before a video was taken of several cycles of contact and separation.

The images taken by the camera were evaluated using image analysis techniques to find the edge pixels. Once these pixels were found for each frame of the video, various curve-fitting techniques were used to determine the radius and center points of the particles, the point of contact of the meniscus with the particle, filling angle, and liquid-solid contact angle.

Data Analysis

Image Processing

Following Bateni et al. (2003), who determined that Laplacian of Gaussian (LoG) filtering was optimal for edge finding when mea-

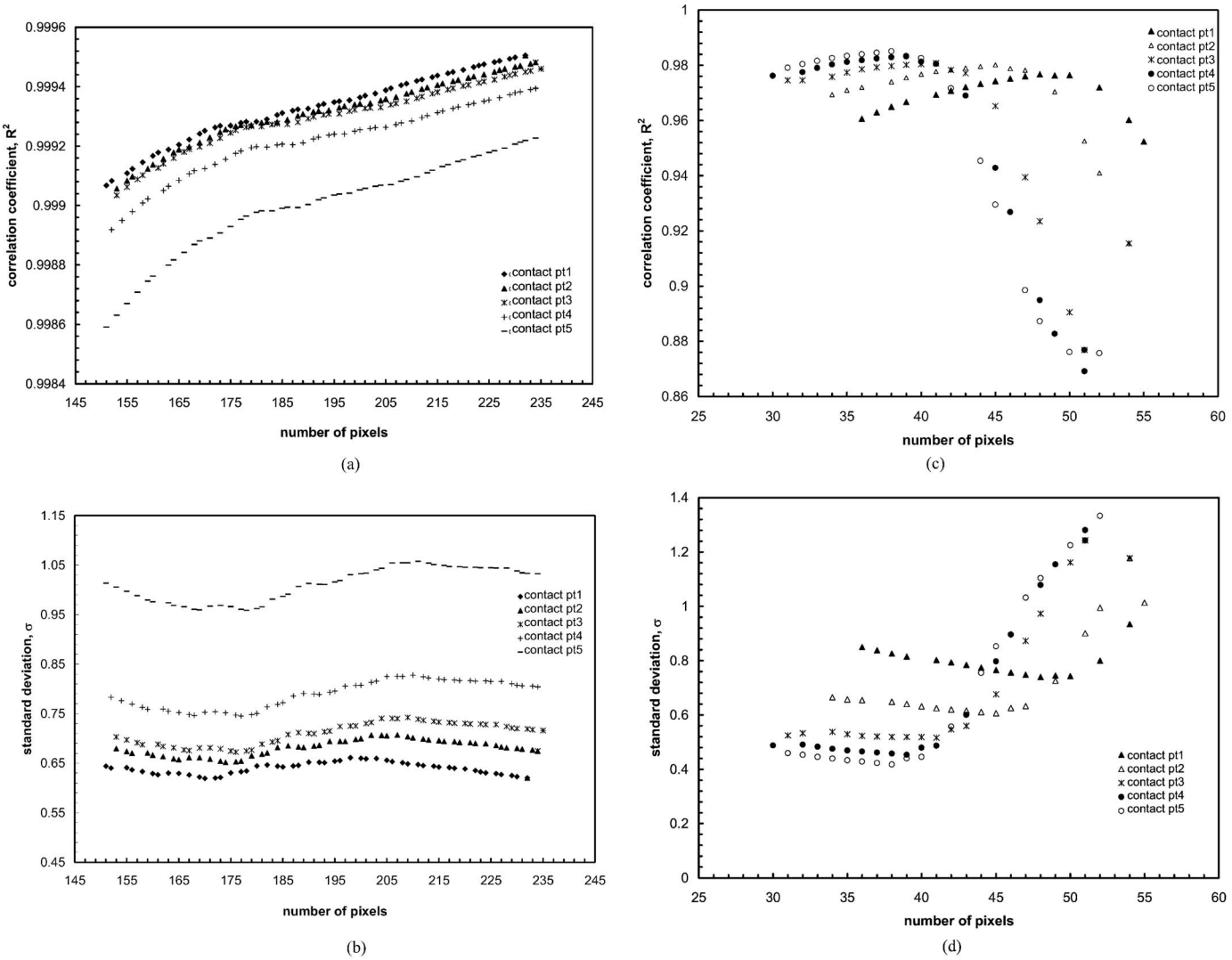

Fig. 6. Quality of fit parameters for circle fit to pixels on left particle in Fig. 3(b). Pixels used were left of guessed particle-meniscus contact point, which was varied over seven different values, xp1–xp5: (a) correlation coefficient, R^2, as function of number of pixels used at various choices of particle-meniscus contact point, xp1–xp5; (b) standard deviation as function of number of pixels used at various choices of particle-meniscus contact point, xp1–xp5; (c) correlation coefficient for second-order polynomial fit to meniscus pixels for varying choice of contact points; and (d) standard deviation for second-order polynomial fit to meniscus pixels for varying choice of contact points.

suring the contact angle of liquid drops on a solid, flat substrate, LoG filtering was used on the gray-scale images taken in the current work to find the edge pixels to be used in the data analysis. The LoG procedure first applies a Gaussian filter to the image to smooth out the gray-scale values of the pixels and then finds the Laplacian or gradient of the gray-scale pixel values. Sharp changes in the gradient indicate boundaries between regions occupied by liquid or solid. Two parameters are used in LoG filtering. These are the width (or number of pixels) used in applying the Gaussian filter kernel and the threshold parameter. A large filter width will smooth out any random noise in the image. The threshold parameter indicates the value of the gradient changes to be taken as indicating the solid edge. The before and after LoG images are shown in Figs. 3(c and d). Notice that the edge finding technique is fairly representative of the edge location that would be determined simply by qualitatively drawing the edge on the raw gray-scale image.

Determining Particle and Meniscus Geometry

Once the edge pixels have been found curve fitting can be used to determine the size of the particles and the shape of the meniscus. Again, based on the method of Betani et al., a range of pixels was chosen and fitted to either a polynomial of varying order or a circle. The type of equation fit to the pixels depended upon the quantity sought.

The deflection of the cantilever particle was measured relative to its stationary position by fitting the equation of a circle to the edge pixels on the left and right of the glass bead. The left and right were chosen since the sides are occupied by either the liquid or the glue supports. To obtain good statistics for the particle parameters, several ranges of pixels were used for curve fitting. The parameters of the circle equations, which yield quality fits as indicated by the correlation coefficient R^2 and the standard deviation σ, are then averaged together. An example of the quality of fit parameters and the circle equation parameters as the number of

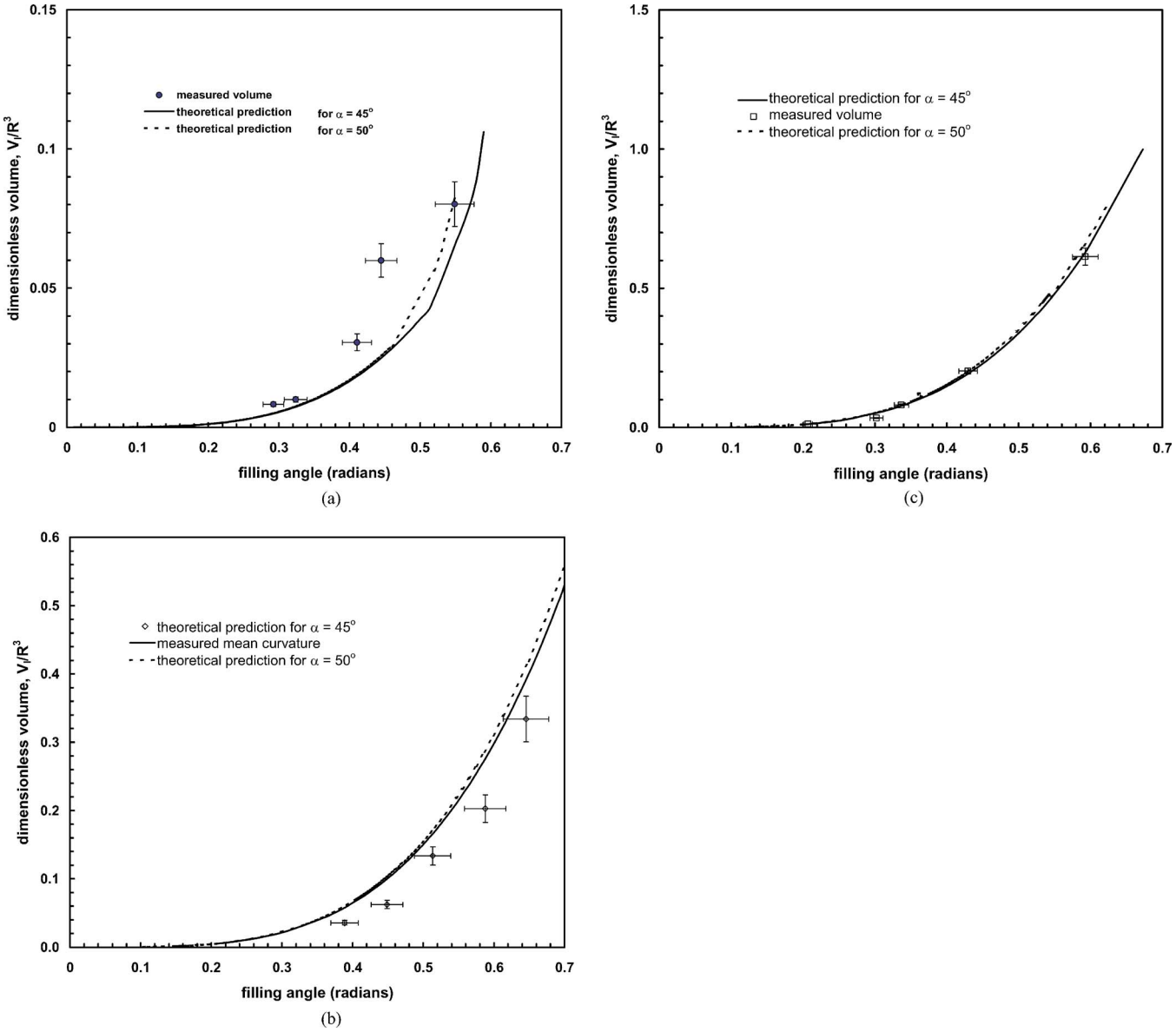

Fig. 7. Comparison of theoretical and experimentally determined dimensionless volume (V_l/R^3)-filling angle (θ) relationship for contact angle, $\alpha=45°$ and $\alpha=50°$, particle size ratios: (a) 1:1 ($R_1=R_2=164$ μm); (b) 1:1.22 ($R_1=164$ μm and $R_2=200$ μm); and (c) 1:1.56 ($R_1=200$ μm and $R_2=255$ μm)

pixels used in the fit increases for the right particle shown in Fig. 3 is shown in Fig. 4. When the number of pixels is small the curvature of the bead is not captured accurately; thus the quality of fit is poor, while at very large numbers of pixels the meniscus pixels and those where the glue connects the particle to the capillary tube or glass fiber begin to be used in the curve fitting again giving poor fits. Notice that as the R^2 value becomes large and stable [Fig. 4(a)] the standard error is relatively low and stable [Fig. 4(b)] and the circle equation parameters (i.e., the center point and the radius) become stable [Figs. 4(c–e)]. Thus, averaging the value of the circle parameters over a range of pixels used in the fit will give a reliable value for the circle parameters. This procedure gives an accurate way to find the same point on each particle repeatedly, i.e., the location of the center of the particle, which can then be tracked from frame to frame by repeating the curve fitting process.

Determining Capillary Forces and Volume of Meniscus

Since the force sought is the force to separate the contacting particles, knowing the deflection of the cantilever at the point when the particles separate is necessary. The point of particle separation can be determined by visually inspecting the gray-scale images or by plotting the distance between particle centers as a function of time (or video frame number) as shown in Fig. 5. It can be seen that initially the distance between particle centers is fairly constant with some statistical fluctuations until about Frames 75–77 when the distance between the particles begins to increase relatively rapidly. Thus Frame 75 plus or minus one frame can be said to represent the point at which the particles separate.

The volume of the liquid applied to the particles can be found most easily by again fitting an equation of a circle to the surface

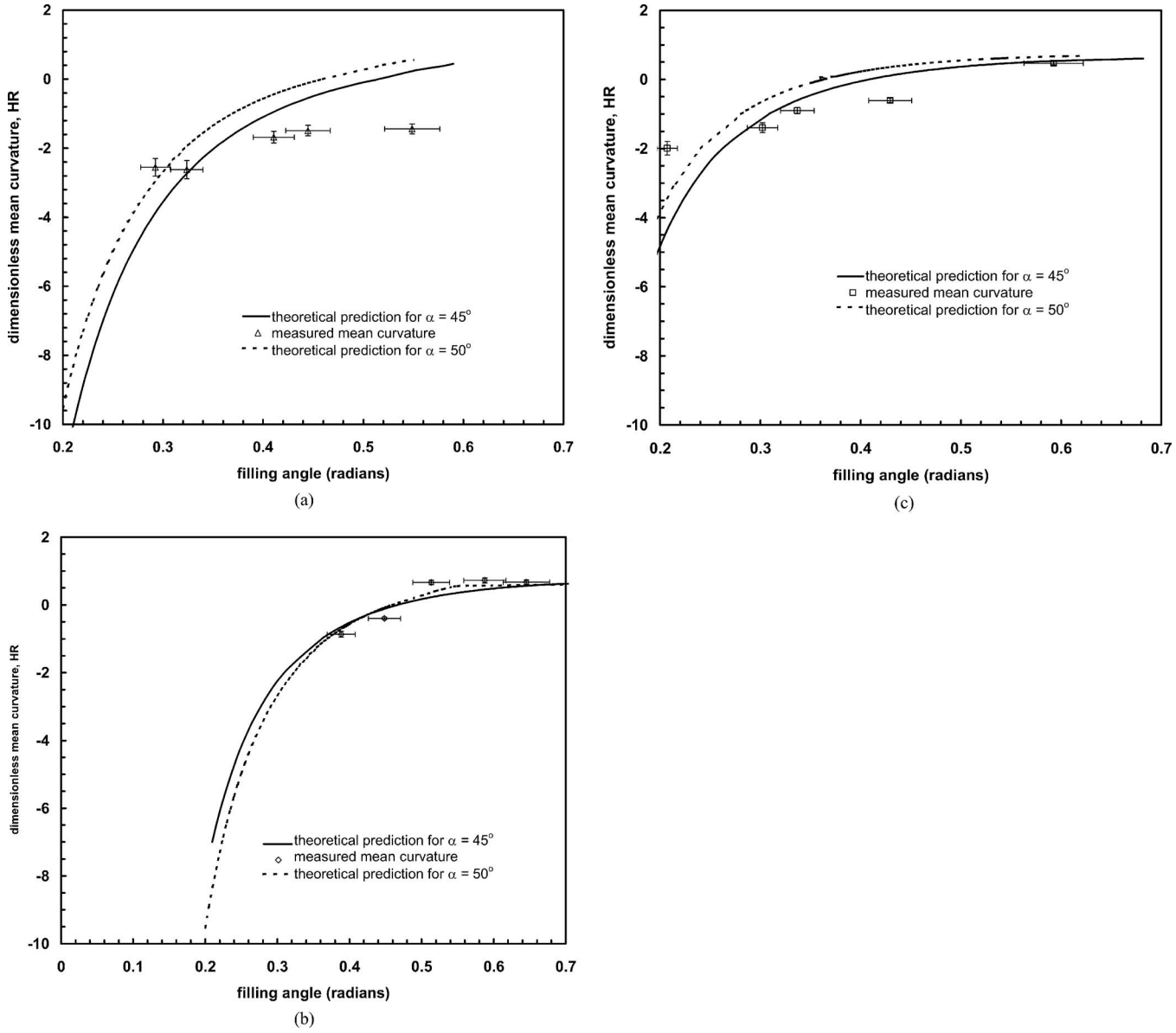

Fig. 8. Comparison of theoretical and experimentally determined dimensionless mean curvature (HR)-filling angle (θ) relationship for contact angle, $\alpha=45°$, and $\alpha=50°$, particle size ratios: (a) 1:1 ($R_1=R_2=164$ μm); (b) 1:1.22 ($R_1=164$ μm and $R_2=200$ μm); and (c) 1:1.56 ($R_1=200$ μm and $R_2=255$ μm)

of the liquid wetting the separated particles, since it is known that the drop assumes a spherical shape under these conditions by others (Rotenberg et al. 1983; Pepin et al. 2000a). The volume can then be calculated from the difference between the volumes of the liquid and spherical particle caps.

Determining Contact Angle and Mean Curvature

The filling angle is measured as the angle from the horizontal (or vertical) to the point of contact between the meniscus and the particle. This point can be found by guessing the approximate point of contact from the raw pixel data and fitting a circle to the particle pixels on one side and a polynomial of varying order, depending on the quality of fit, to the meniscus pixels on the other. The intersection of the two curves gives the contact point and the filling angle can be measured from there. Varying the initial guess of the point of contact gives an additional way to assess whether a good value of the point of contact has been found. Fig. 6 shows an example of the quality of fit parameters for the circle fit to the particle pixels [Figs. 6(a and b)] and for a second-order polynomial fit to the meniscus pixels [Figs. 6(c and d)], for a varying choice of meniscus-particle contact point, labeled contact point 1–5 in the figure. Notice that as the contact point changes and the meniscus pixels begin to be included in the circle fit to the particle, the quality of fit decreases, while the quality of fit to the meniscus pixels becomes poor as the particle pixels are included. The point of contact can then be estimated as the last point where the R^2 value is still relatively high and the standard error is low for both the circle fit to the particle and the polynomial fit to the meniscus (e.g., contact point 3 is a good choice in Fig. 6). The contact angle between the liquid and the solid can then be determined from the slope of the fit curves at the intersection point. The value of the contact angle

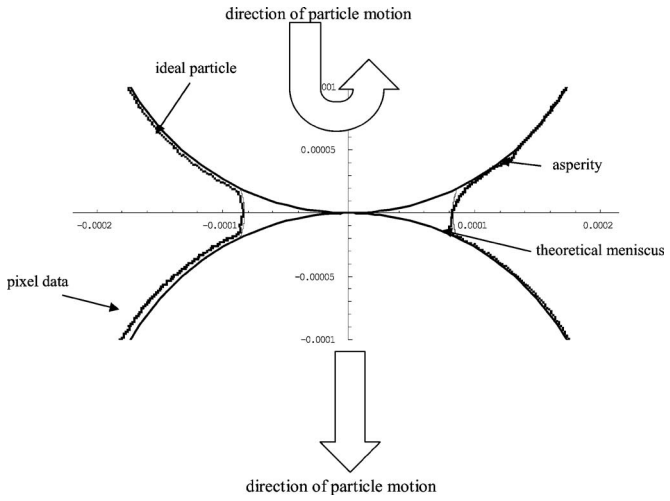

Fig. 9. Comparison of theoretical, identical, two-particle meniscus with experimental data taken from frame just prior to separation: $R=200$ μm, contact angle $\alpha=\pi/4$

was determined to be about $\pi/4$, which is in the range of advancing and receding contact angles determined by others (see e.g., Pepin et al. 2000a). However, particularly for small liquid contents, obtaining good statistics for the contact angle was difficult due to the lack of a wide range of pixels to be used in the curve fitting and contact point pinning effects (see Fig. 9 and discussion below). Therefore, experimental results shown will be compared to theoretical results where two values of contact angle, 45 and 50°, have been used in order to show that the experimental results are bracketed by this range of contact angles.

To determine the mean curvature of the meniscus and thus the matric suction [see Eq. (1)] further care must be taken. For axisymmetric menisci the Laplace equation for profiles can be written as

$$2H = \frac{\Delta u}{\sigma_{la}} = \frac{1}{r(1+\dot{r}^2)^{1/2}} - \frac{\ddot{r}}{(1+\dot{r}^2)^{3/2}} \tag{5}$$

where $\cdot$ implies the spatial derivative d/dz. Since the mean curvature $H=$constant for these surfaces, Eq. (5) must hold over the entire profile and in particular at the end points. Thus, making the substitution $Y=(1+\dot{r}^2)$ into Eq. (5) and rearranging gives a Bernouilli type differential equation (see e.g., De Bisschop and Rigole 1982; Lian et al. 1993)

$$\frac{dY}{dr} - \frac{2Y}{r} = \frac{2\Delta u}{\sigma_{la}} Y^{3/2} \tag{6}$$

which can be integrated to give

$$\frac{r}{(1+\dot{r}^2)^{1/2}} + \frac{\Delta u}{2\sigma_{la}} r^2 = C \tag{7}$$

where $C=$integration constant to be determined from the boundary conditions. At the point of contact between the left particle (implied by the subscript ct) and meniscus [see Fig. 1(b)]

$$z(r_{ct}) = R_1(1+\cos\theta) \tag{8}$$

$$r(z_{ct}) = R_1 \sin\theta \tag{9}$$

$$\left.\frac{dr}{dz}\right|_{z_{ct}} = \cot(\theta+\alpha) \tag{10}$$

so that Eq. (7) can be solved for uneven-sized spheres by considering only the points of contact between the particles and the meniscus to give

$$\frac{\Delta u}{2\sigma_{la}} = \frac{r_{ct}\sin(\theta+\alpha) - r_{cb}\sin(\gamma+\alpha)}{r_{ct}^2 - r_{cb}^2} \tag{11}$$

where $r_{ct}(r_{cb})=r$ coordinate of the contact point between the meniscus and the left (or right) particle. For even-sized particles the radius of the meniscus at the point of contact between the particles must be used. Now the matric suction can be calculated based on the filling angles on the left and right particles and the location of the contact points.

Experimental Results

Recall that posing the two-particle meniscus problem requires the minimum energy of the system to be found [see Eq. (2)]. In essence this reduces to finding the minimum surface area of the liquid-gas interface at constant volume. The Lagrange multiplier (matric suction) can then be determined as well as the location of the contact points of the meniscus on the particle. Thus, in the way the problem is approached theoretically, there is only one independent variable (i.e., here the liquid volume). In the current experimental procedure the liquid volume is controlled while the end points, through the filling angle, θ, and the matric suction are left to find the values that would minimize the free energy of the system. The assumption of variable end points implies that the particles are smooth and that contact point "pinning," where the meniscus particle contact point is fixed due to local roughness, does not occur. Since the particles used in the experiments were rough, it is necessary at the outset to verify that contact point pinning is not a significant factor. This can be done by comparing the theoretical filling angle-volume relationship against those obtained experimentally.

Volume versus Filling Angle

Fig. 7 shows the results of experiments with particles of size ratios 1:1, 1:1.22, and 1:1.56, compared to the theoretical values. The radii of the smaller particles in the experiments were 164 μm [Figs. 7(a and b)] and 200 μm [Fig. 7(c)] while the contact angle used was $\pi/4$. These values are the same for all the results shown in this section. It can be seen in Fig. 7 that, in general, the experimentally determined values follow the same qualitative pattern as the theoretical values, and especially for size ratio 1:1.56 [Fig. 7(c)] are close to the theoretical values. The discrepancy in the results of the size ratio 1:1 case [Fig. 7(a)] may be explained by reference to the fact that the particles used were not exactly identical as can be seen in Fig. 9 (see discussion below).

Mean Curvature versus Filling Angle

A further check on the validity of the theory by the experiments can be seen in Fig. 8, where the relationship between the mean curvature and filling angle is shown. Again, the qualitative agreement is good and the quantitative comparison appears better than in the volume case. Discrepancies in the theoretical and experimental values can be understood by reference to Fig. 9.

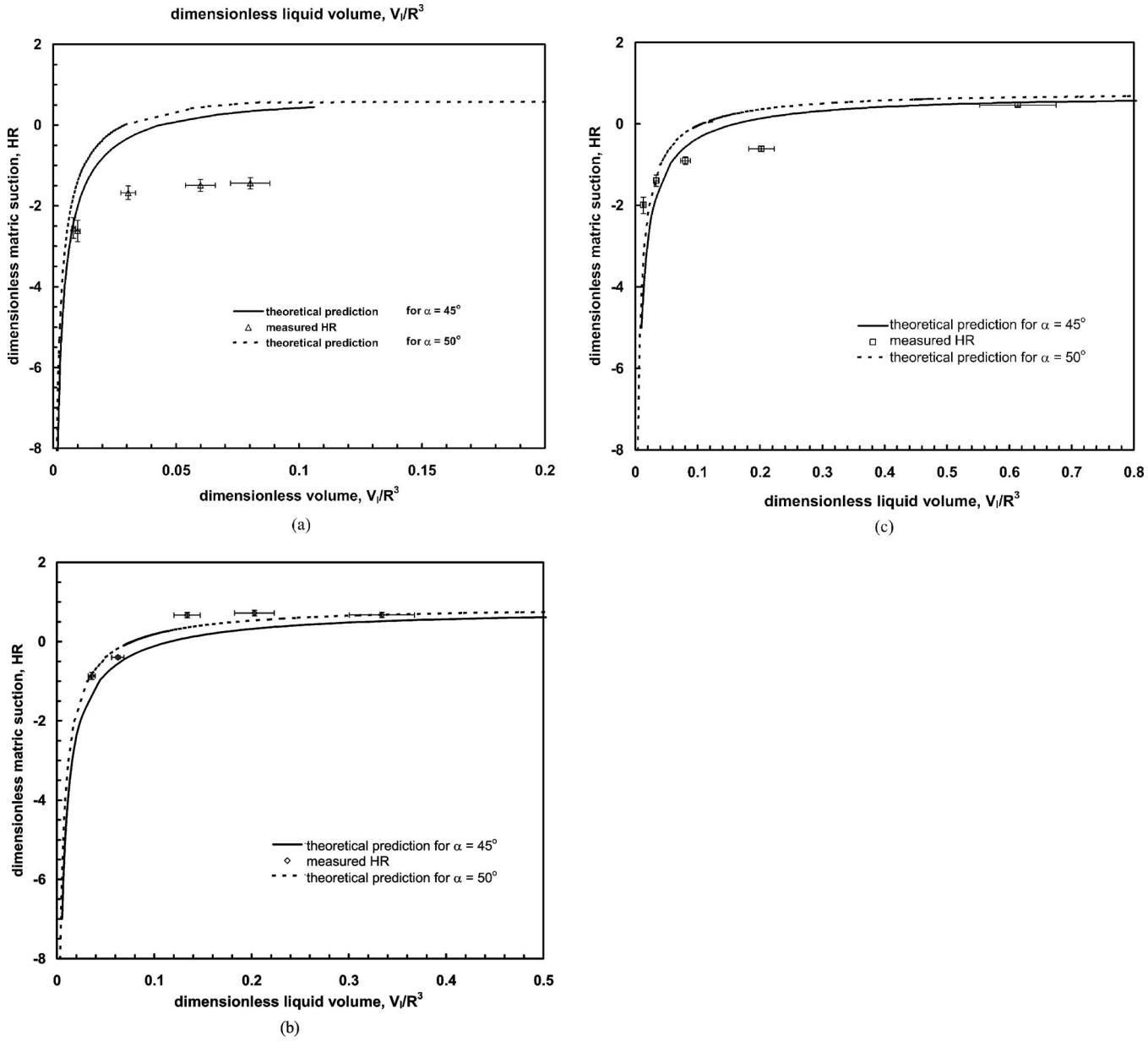

Fig. 10. Comparison of theoretical and experimentally determined dimensionless solid water characteristic curves (SWCC) for contact angle, $\alpha=45°$, and $\alpha=50°$, particle size ratios: (a) 1:1 ($R_1=R_2=164$ μm); (b) 1:1.22 ($R_1=164$ μm and $R_2=200$ μm); and (c) 1:1.56 ($R_1=200$ μm and $R_2=255$ μm)

Fig. 9 shows a comparison between the raw pixel data for the meniscus between two particles with size ratio 1:1 and the theoretically calculated meniscus shape. The configuration shown in Fig. 9 corresponds to a filling angle of 0.455 rad and the pixel data come from the frame just prior to particle separation. The frame at which the edge pixel data are determined is important because there can be relative movement of the particles, even though they remain in contact. Thus, on the right of Fig. 9, the meniscus is deformed due to the relative movement of the particles and the apparent pinning of the contact point at the asperity on the left particle. On the left particle a receding contact angle may be more appropriate while on the bottom particle of the right side an advancing angle may be appropriate. Also, notice that the meniscus on the left side is relatively unaffected. Moreover, note the other nonidealities occur in the system. The particles are not identically sized or perfectly spherical, etc. In general, these nonidealities can at least partially explain the differences between the theoretical and experimental values.

Solid-Water Characteristic Curve

Now that the volume and mean curvature have been found they can be combined to show what is called the SWCC, which is the matric suction in the soil as a function of water content. The SWCC for the theoretical two particle systems considered here are shown in Fig. 10 along with the experimentally determined data. The same trends can be noted as above. Also, note that the liquid contents used fall in large part in the negative, or repulsive, matric suction range for the size ratio 1:1.22 case. Referring back to Fig. 8, it can be seen that these repulsive matric suctions occur

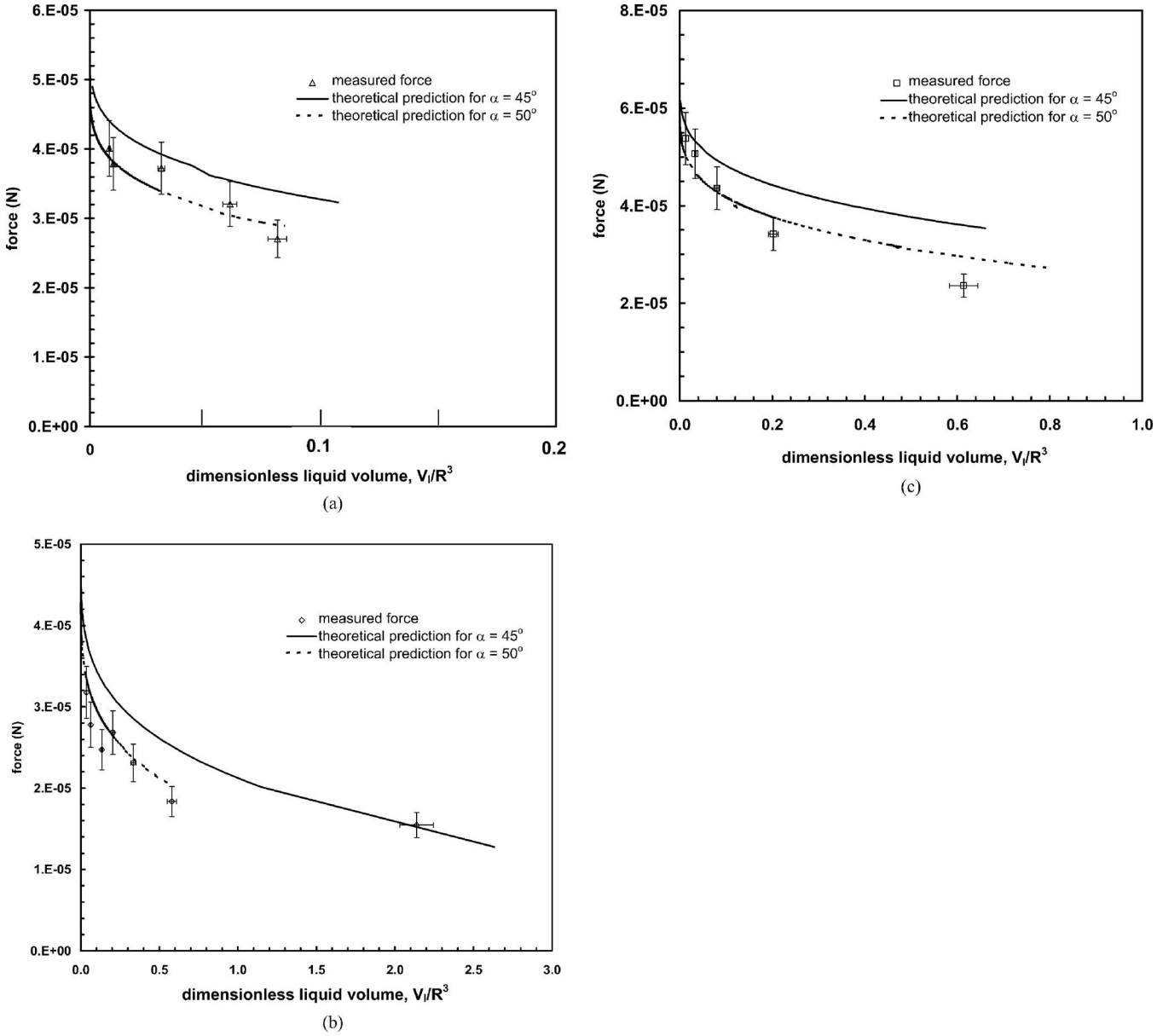

Fig. 11. Comparison of theoretical and experimentally determined capillary force characteristic curves (CFCC) for contact angle, $\alpha=45°$, and $\alpha=50°$, particle size ratios: (a) 1:1 ($R_1=R_2=164$ μm); (b) 1:1.22 ($R_1=164$ μm and $R_2=200$ μm); and (c) 1:1.56 ($R_1=200$ μm and $R_2=255$ μm)

below a filling angle of $\pi/4$. This means that in a simple cubic packing of these particles, where particle-pair menisci are isolated below filling angles of $\pi/4$, one would expect negative matric suctions to be important.

Capillary Force Characteristic Curve

Finally, the comparison of the capillary force characteristic curves for the particle size ratios can be seen in Fig. 11. It should be noted that the force measured here is the force required to separate the particles that are initially in contact. In general the force as a function of particle separation can be determined, but one must account for the viscosity of the liquid (Mathewson 1988) and contact angle hysteresis (Pepin et al. 2000a; Rosetti et al. 2003). The results shown in Fig. 11 indicate good qualitative agreement between the measured and theoretical results. The experimental results are bracketed by contact angles of 45 and 50°.

Conclusions

A novel micromechanical testing technique has been applied to measure the force required to separate two particles of varying size ratios with a liquid bridge between them. Computational techniques for calculating the volume, mean curvature of the meniscus, and capillary force are established. The experimental results have been compared to theoretical results. The variable endpoint assumption used in the theory was assessed and shown to be in good qualitative agreement with the experiments. In addition, the SWCC for the two-particle systems was determined experimentally. Repulsive (negative) matric suctions were shown to be potentially significant. The CFCC was also experimentally determined for various particle size ratios. For the contact angle and particle radii used, it can be seen that the theory predicts the magnitudes of the capillary force and water retention quite well.

Nonidealities such as advancing and receding contact angles, meniscus particle contact point pinning, etc. may partially explain the observed discrepancies between theoretical prediction and experimental results.

Acknowledgments

The writers would like to express their gratitude to Ms. Sarunya Promkotra for many useful discussions on how to set up the experimental program. Partial funding for this research provided by Petroleum Research Fund of American Chemical Society (Grant No. 42688-AC9) to N.L. is greatly appreciated.

References

Bateni, A., Susnar, S. S., Amirfazli, A., and Neumann, A. W. (2003). "A high-accuracy polynomial fitting approach to determine contact angles." *Colloids Surf., A*, 219, 215–231.

De Bisschop, F. R. E., and Rigole, W. J. L. (1982). "A physical model for liquid capillary bridges between adsorptive solid spheres: The nodoid of plateau." *J. Colloid Interface Sci.*, 88, 117–128.

Eccleston, K. L., and Miller, K. T. (2002). "Direct measurement of strongly attractive particle-particle interactions." Improved ceramics through new measurements, processing, and standards, *Ceram. Trans.*, 133, 33–38.

Erle, M. A., Dyson, D. C., and Morrow, N. R. (1971). "Liquid bridges between cylinders, in a torus, and between spheres." *AIChE J.*, 17, 115–121.

Forsyth, W. E. (2003) *Smythsonian physical tables*, 99th revised Ed., Table 555, Knovel, Norwich, N.Y.

Lechman, J. B., and Lu, N. (2008). "Capillary force and water retention between two uneven-sized particles." *J. Eng. Mech.*, 135(5), 374–384.

Lian, G., Thorton, C., and Adams, M. J. (1993). "A theoretical study of the liquid bridge forces between two rigid spherical bodies." *J. Colloid Interface Sci.*, 161, 138–147.

Mason, G., and Clark, W. C. (1965). "Liquid bridges between spheres." *Chem. Eng. Sci.*, 20, 859–866.

Mathewson, M. J. (1988). "Adhesion of spheres by thin liquid films." *Philos. Mag. A*, 57, 207–216.

McFarlane, J. S., and Tabor, D. (1950). "Adhesion of solids and the effect of surface films." *Proc. R. Soc. London, Ser. A*, 202, 224–241.

Melrose, J. C. (1966). "Model calculations for capillary condensation." *AIChE J.*, 12, 986–994.

Miller, C. A., and Neogi, P. (1985). *Interfacial phenomena: Equilibrium and dynamic effects*, Marcel Dekker, New York.

Molenkamp, F., and Nazemi, A. H. (2003). "Interactions between two rough spheres, water bridge and water vapor." *Geotechnique*, 53, 255–264.

Orr, F. M., Scriven, L. E., and Rivas, A. P. (1975). "Pendular rings between solids: meniscus properties and capillary force." *J. Fluid Mech.*, 67, 723–742.

Pepin, X., Rossetti, D., Iveson, S. M., and Simons, S. J. R. (2000a). "Modeling the evolution and rupture of pendular liquid bridges in the presence of large wetting hysteresis." *J. Colloid Interface Sci.*, 232, 289–297.

Pepin, X., Rossetti, D., and Simons, S. J. R. (2000b). "Modeling the evolution and rupture of pendular liquid bridges in the presence of large wetting hysteresis." *J. Colloid Interface Sci.*, 232, 298–302.

Rossetti, D., Pepin, X., and Simons, S. J. R. (2003). "Rupture energy and wetting behavior of pendular liquid bridges in relations to the spherical agglomeration process." *J. Colloid Interface Sci.*, 261, 161–169.

Rotenberg, Y., Boruvka, L., and Neumann, A. W. (1983). "Determination of surface tension and contact angle from the shapes of axisymmetric fluid interfaces." *J. Colloid Interface Sci.*, 93, 169–183.

Washburn, E. W. (2003). *International critical tables of numerical data, physics, chemistry and technology*, 1st Electronic Ed., Vol. 5, Knovel, Norwich, N.Y., 450.